Isotope Effect on Energy Confinement Time and Thermal Transport in Neutral-Beam-Heated Stellarator-Heliotron Plasmas

H. Yamada,[1,2] K. Tanaka,[1,3] R. Seki,[1,4] C. Suzuki,[1] K. Ida,[1] K. Fujii,[5] M. Goto,[1,4] S. Murakami,[5] M. Osakabe,[1,4] T. Tokuzawa,[1,4] M. Yokoyama,[1,4] M. Yoshinuma,[1] and LHD Experiment Group[1]

[1]*National Institute for Fusion Science, National Institutes of Natural Sciences, Toki, Gifu 509-5292, Japan*
[2]*The University of Tokyo, Kashiwa, Chiba 277-8568, Japan*
[3]*Kyushu University, Kasuga, Fukuoka 816-8580, Japan*
[4]*SOKENDAI (The Graduate University for Advanced Studies), Toki, Gifu 509-5292, Japan*
[5]*Kyoto University, Kyoto 615-8530, Japan*

(Received 2 July 2019; revised manuscript received 30 August 2019; published 29 October 2019)

The isotope effect on energy confinement time and thermal transport has been investigated for plasmas confined by a stellarator-heliotron magnetic field. This is the first detailed assessment of an isotope effect in a stellarator heliotron. Hydrogen and deuterium plasmas heated by neutral beam injection on the Large Helical Device have exhibited no significant dependence on the isotope mass in thermal energy confinement time, which is not consistent with the simple gyro-Bohm model. A comparison of thermal diffusivity for dimensionally similar hydrogen and deuterium plasmas in terms of the gyroradius, collisionality, and thermal pressure has clearly shown robust confinement improvement in deuterium to compensate for the unfavorable mass dependence predicted by the gyro-Bohm model.

DOI: 10.1103/PhysRevLett.123.185001

It has been recognized that thermal transport in a magnetically confined toroidal plasma is dominated by the turbulence which has the characteristic scale of an ion gyroradius. This model is referred to as the gyro-Bohm model and is successful in many experiments [1,2]. Theoretical studies on drift turbulence also support these experimental observations. It should be noted that the ion gyroradius is proportional to the square root of the mass. Therefore, a plasma with a heavier hydrogenic isotope would have a larger thermal diffusivity according to this gyro-Bohm model. However, major experimental observations have shown better performance and, hence, better confinement for a deuterium plasma than a hydrogen plasma (see, e.g., Refs. [3,4]). This isotope effect is not consistent with the gyro-Bohm model and remains a long-standing mystery in fusion plasma research. Clarification of the origin of the isotope effect is a key issue to project a fusion reactor which uses deuterium and tritium as fuel.

The gyro-Bohm model defines the thermal diffusivity χ scaled by $\rho_*\chi_B$. Here ρ_* is the ion gyroradius normalized by the plasma minor radius a and χ_B is the Bohm diffusivity, $\chi_B = T/(eB)$, where T, e, and B are the temperature, elementary charge, and magnetic field, respectively. Consequently, the energy confinement time τ_E normalized by ion cyclotron frequency Ω_i is scaled with ρ_*^{-3} [1]. Indeed, a representative scaling for tokamaks, IPB$(y,2)$ [5] shows in dimensionless form: $\tau_E^{\mathrm{IPB98}(y,2)}\Omega_i \propto \rho_*^{-2.70}$, which is close to the gyro-Bohm model. Plasmas confined only by an external magnetic field such as a stellarator and heliotron have exhibited similar dependence such as $\tau_E^{\mathrm{ISS04}}\Omega_i \propto \rho_*^{-2.79}$ [6], which suggests a commonality of toroidal plasmas. Local thermal diffusivity in a stellarator heliotron has also shown characteristics consistent with the gyro-Bohm model in a dimensionally similar comparison of hydrogen plasmas with different magnetic field strengths [7,8]. Unlike the tokamak, however, a discussion of an isotope effect in a stellarator heliotron [9,10] remains premature, and a recent experiment on the Large Helical Device (LHD) [11] has enabled the first detailed assessment of an isotope effect by comparing hydrogen and deuterium plasmas [12].

In this study, only uneventful plasmas heated by neutral-beam injection (NBI) in a quasisteady state without a dynamical transition and formation of a spatial transport barrier have been assessed. The surveyed range of physical parameters such as B, $\bar{n}_e$ (line averaged density), P_{abs} (absorbed heating power), and I_p (plasma current) are summarized in Table I. While the net toroidal plasma current up to several tens kA is driven by NBI and bootstrap, its effect on the magnetohydrodynamics equilibrium property is negligible, since the rotational transform generated by an external helical field is equivalent to the plasma current of 2 MA at 2.75 T. Since the used NBI has an accelerating voltage as high as 180 kV, electron heating is predominant, i.e., $P_{\mathrm{abs}}^e > P_{\mathrm{abs}}^i$. Consequently, the central electron temperature T_{e0} is higher than the central ion temperature T_{i0}. Data clusters of hydrogen and deuterium plasmas are well separated in terms of the isotope density fraction of $n_{\mathrm{D}}/(n_{\mathrm{H}} + n_{\mathrm{D}})$, which is evaluated by

 © 2019 American Physical Society

TABLE I. Parameter regimes of hydrogen and deuterium plasmas. Ranges are shown by minimum and maximum, and ratios are shown by average and standard deviation.

	H	D
Range		
B (T)	1.64–2.75	1.375–2.75
$\bar{n}_e$ (10^{19} m^{-3})	0.67–4.32	0.64–5.7
$P_{\rm abs}$ (MW)	1.8–11.7	1.5–12.5
I_p (kA)	−54– + 40	−50– + 26
Ratio		
$P^e_{\rm abs}/P^i_{\rm abs}$	3.76 ± 1.64	4.36 ± 2.21
T_{e0}/T_{i0}	1.63 ± 0.36	1.79 ± 0.32
$n_{\rm D}/(n_{\rm H}+n_{\rm D})$	0.09 ± 0.03	0.94 ± 0.03
$Z_{\rm eff}$	1.30 ± 0.16	1.38 ± 0.09

H_α and D_α emissions. The radial position of the vacuum magnetic axis $R_{\rm ax}$, which characterizes the magnetic configuration in the LHD, is fixed at 3.6 m. Plasma equilibrium is reconstructed by VMEC [13], and FIT3D [14] and TASK3D-a [15,16] are used for the analysis of absorbed heating power and power balance. Fast ion loss due to energetic-particle-driven instabilities [17] has not been observed in the plasmas analyzed in this study. Thermal stored energy has been evaluated by profiles documented by means of Thomson scattering and charge exchange recombination spectroscopy. Dilution of ions due to major impurities of helium and carbon is also taken into account.

A statistical regression analysis has yielded a scaling expression in operational parameters:

$$\tau^{\rm scl}_{E,\rm th} = 0.072 M^{0.00\pm0.02} B^{0.84\pm0.02} \bar{n}_e^{0.76\pm0.01} P_{abs}^{-0.87\pm0.01}, \quad (1)$$

where the mass number M is simply set at 1 for hydrogen and 2 for deuterium. The units of $\tau^{\rm scl}_{E,\rm th}$, B, $\bar{n}_e$, and $P_{\rm abs}$ are s, T, 10^{19} m^{-3}, and MW, respectively. A comparison of experiment data with the prediction by this scaling is shown in Fig. 1. This expression gives a remarkable good fitting with the root mean square error of only 3%. It is noted that a dependence on the density and heating power has been found to be stronger than the previous study [6], where the absorbed heating power was limited to half (around 6 MW) of the present dataset. Here no dependence on the mass of isotopes is identified. This result is similar to the result of a type I ELMy H mode on the Joint European Torus [18]. Here it should be noted that the expression of (1) appears to be inconsistent with the gyro-Bohm model which accounts for $M^{-0.5}$ dependence. When the energy confinement time normalized by the ion gyrofrequency [1] is assumed to be expressed only by four dimensionless parameters such as ρ_*, ν_* (electron-ion collision frequency normalized by the bounce frequency in a banana orbit), β (plasma thermal pressure normalized by the pressure of a magnetic field) and M, the scaling (1) is rephrased into the following dimensionless expression:

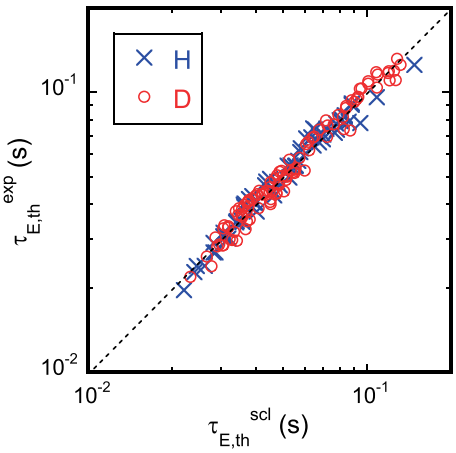

FIG. 1. Comparison of the thermal energy confinement time in the experiment and the prediction by the scaling. Crosses and circles are hydrogen plasmas and deuterium plasmas, respectively.

$$\tau^{\rm scl}_{E,\rm th}\Omega_i \propto M^{0.99}\rho_*^{-2.98}\nu_*^{0.19}\beta^{-0.30}. \quad (2)$$

Here a clear mass dependence is identified, which compensates for the unfavorable negative dependence on the mass in the gyro-Bohm model. At the same time, it should be emphasized that the gyro-Bohm dependence of ρ_*^{-3} persists.

Then, thermal diffusivity in dimensionally similar plasmas is compared in order to clarify the peculiarity of the isotope effect seen in the energy confinement time. Since the three operational parameters that are B, $\bar{n}_e$, and $P_{\rm abs}$ are controllable in the experiment, dimensionally similar (more strongly identical) conditions in terms of ρ_*, ν_*, and β can be fulfilled for plasmas with different masses, namely, hydrogen and deuterium plasmas. Provided the gyro-Bohm nature except for the mass dependence is assumed for the energy confinement time with using the confinement improvement factor of α ($= \tau_E^{\rm D}/\tau_E^{\rm H}$), which is unknown, the operational conditions to enable a comparison of dimensionally similar plasmas with hydrogen and deuterium are derived by the following relation with the mass ratio between hydrogen and deuterium of 2 [19,20]: $B_{\rm D} = 2^{3/4}B_{\rm H}$, $n_{\rm D} = 2n_{\rm H}$, $P^{\rm D}_{\rm abs} = 2^{3/4}\alpha^{-5/2}P^{\rm H}_{\rm abs}$. The comparison of hydrogen plasmas at 1.64 T with deuterium plasmas at 2.75 T is highlighted. Since α is unknown, heating power has been scanned to get temperatures with a factor of $\sqrt{2}$ difference. It should be noted that the gyro-Bohm model corresponds to α of $1/\sqrt{2}$. Figure 2 shows the (a) electron and (b) ion temperature and (c) electron density profiles in a typical pair of dimensionally similar plasmas. These parameters are normalized by the mass ratio to confirm the matching for dimensional similarity. Here attention should be paid to the difference of physics

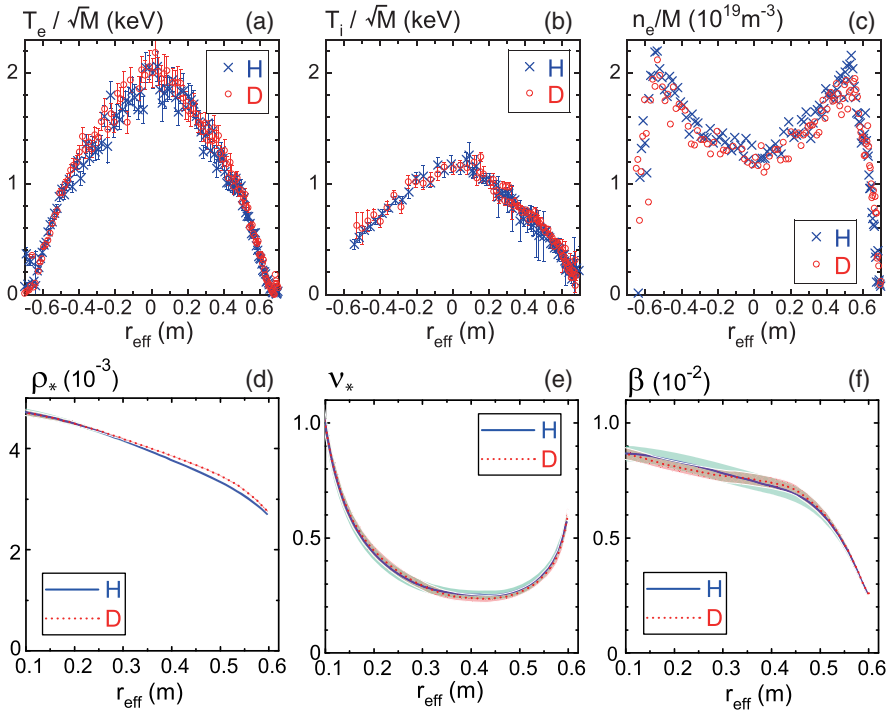

FIG. 2. Profiles of dimensionally similar hydrogen and deuterium plasmas. r_{eff} is the effective minor radius, and the last closed flux surface is located at $r_{\mathrm{eff}} = 0.63$ m. The negative and positive signs mean the inboard side and the outboard side with respect to the magnetic axis, respectively. (a) The electron temperature, (b) ion temperature, and (c) electron density in the top panels. Data of hydrogen plasma and deuterium plasma are shown by crosses and circles, respectively. (d) The normalized gyroradius, (e) normalized collisionality, and (f) normalized pressure in the bottom panels. Data of hydrogen plasma and deuterium plasma are shown by solid and dashed curves, respectively.

processes in the core and the edge regions. For example, deeper neutral penetration is suggested in H than in D due to the larger thermal velocity. The e-folding length of neutral penetration in the edge region is evaluated at 4.1 and 3.4 cm for hydrogen and deuterium [21], respectively. However, the density profile matches towards the very edge fortuitously. Corresponding profiles of dimensionless parameters are shown in Figs. 2(d)–2(f). Remarkable matching has been successfully obtained.

The required power ratio $P_{\mathrm{abs}}^{\mathrm{D}}/P_{\mathrm{abs}}^{\mathrm{H}}$ in this pair is 1.71, which corresponds to α of 0.99, showing no difference between hydrogen and deuterium. This observation is consistent with the scaling of energy confinement time (1). Since these two plasmas are identical in terms of ρ_*, ν_*, and β, the thermal diffusivity normalized by the cyclotron frequency should be the same according to whichever neoclassical, Bohm, or gyro-Bohm models. Since this study focuses on the magnetic configuration which suppresses neoclassical helical ripple transport, turbulent transport is in excess of neoclassical transport.

Figure 3 shows the comparison of thermal diffusivity in dimensionally similar plasmas shown in Fig. 2. A difference between hydrogen and deuterium is evident even considering the range of the error. The electron channel is improved significantly in the deuterium plasma compared with the hydrogen plasma. The improvement in the ion channel is less than in the electron channel. However, a difference between hydrogen and deuterium is still observable. The improvement in heat diffusivity is robustly seen in the entire radius, which compensates for degradation due to the gyro-Bohm factor $(1/\sqrt{2})$ in the energy confinement time.

Among the compiled database, 15 pairs of dimensionally similar plasmas have been investigated. Figure 4(a) shows

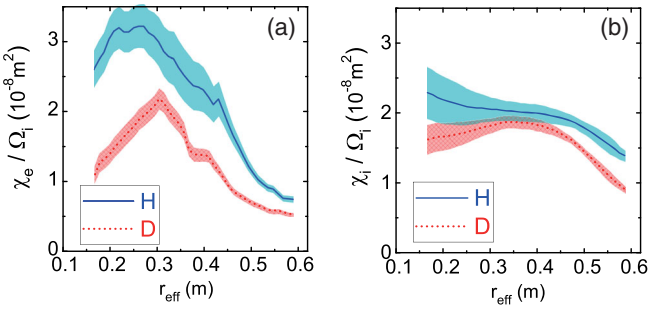

FIG. 3. Comparison of the thermal diffusivity in a pair of dimensionally similar hydrogen (solid curves) and deuterium (dashed curves) plasmas shown in Fig. 2. Thermal diffusivity is normalized by the ion cyclotron frequency. (a) Electron thermal diffusivity and (b) ion thermal diffusivity.

the ratio of normalized thermal diffusivity (the ratio of dashed curves for deuterium to solid curves for hydrogen in Fig. 3) at $\rho = 2/3$ as a function of the collisionality. It is seen that the ratio of electron thermal diffusivity robustly stays at around 0.5, which may implicate $1/M$. The ratio of ion thermal diffusivity shows a different trend. Although it is also less than 1 in the low collisionality regime, it approaches 1 as the collisionality increases. One important element in the comparison of thermal transport in hydrogen and deuterium plasma is the difference in the collisional electron-ion energy exchange [22]. Heat transfer between electrons to ions P_{ei} is proportional to $n^2(T_e - T_i)/(MT_e^{3/2})$. Since $T_e > T_i$ in plasmas studied here, it is expected that an enhancement of P_{ei} in hydrogen plasmas leads to the increase of ion heat flux. Therefore, each contribution of ion and electron loss channels to the total heat flux, namely, net confinement, should be assessed. Figure 4(b) shows the ratio of the electron heat flux q_e to the ion heat flux q_i at $\rho = 2/3$ corresponding to the data plotted in Fig. 4(a). While the electron heat flux decreases with the increase of collisionality ($\nu_* \propto n/T^2$) through the enhancement of electron-ion energy transfer, this trend is less pronounced in hydrogen plasmas than in deuterium plasmas. This is because the density is set at double for a deuterium plasma in this comparison and the effect of mass on the electron-ion energy transfer is canceled out. The electron loss channel stays dominant, in particular, in hydrogen plasmas, and the ion loss channel does not become dominant. Therefore, the improvement of thermal diffusivity in deuterium shown in Fig. 4(a) leads to the significant mass dependence ($\propto M^{0.99}$) seen in the scaling expression in dimensionless parameters (2).

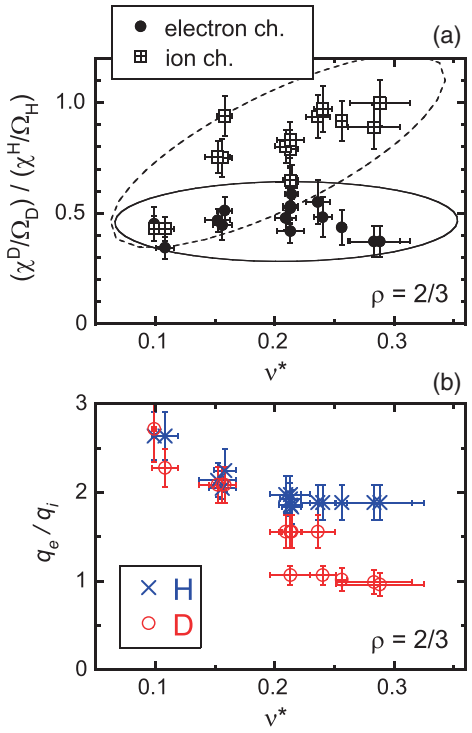

FIG. 4. Comparison of the thermal transport in pairs of dimensionally similar hydrogen and deuterium plasmas. (a) The ratio of thermal diffusivity in a deuterium plasma to that in a hydrogen plasma at $\rho(= r_{\rm eff}/a) = 2/3$ as a function of the collisionality. Open and closed circles are the electron heat loss channel and ion heat loss channel, respectively. Ellipses are 95% probability. (b) The ratio of electron heat flux to ion heat flux at $\rho = 2/3$ as a function of the collisionality. Crosses and open circles are hydrogen and deuterium plasmas, respectively.

NBI heated hydrogen and deuterium plasmas in the LHD do not show different performance at the same operational parameters under the condition of dominant electron heating. This observation is not consistent with the prediction by the gyro-Bohm model. The dimensionless expression of the scaling of the energy confinement time suggests the persistence of mass dependence and the gyro-Bohm nature, $\tau_{E,\rm th}^{\rm scl}\Omega_i \propto M^{0.99}\rho_*^{-2.98}$. A clarification of the underlying physics of this mass dependence is the next challenge. A careful comparison of thermal transport in dimensionally similar hydrogen and deuterium plasmas with different M has shown robust improvement of thermal diffusivity, in particular, in the electron heat loss channel in deuterium plasmas, which is consistent with the identified characteristics of the energy confinement time. While a theoretical model for an isotope effect is becoming matured in a tokamak [23], an elaborate comparison of a tokamak and a stellarator heliotron could lead to a comprehensive understanding of this elusive but important physics issue.

One of the authors (H. Y.) acknowledges technical assistance by Ms. K. Hashimoto, valuable communications with Dr. C. F. Maggi, and the long-standing encouragement by Professor F. Wagner. The authors express their deepest gratitude to the late Professor S.-I. Itoh for her continuous support of this study. This work is supported by the National Institute for Fusion Science grant administrative budgets (NIFS19KLPH038 and NIFS17UNTT008).

[1] T. C. Luce, C. C. Petty, and J. G. Cordey, Plasma Phys. Controlled Fusion **50**, 043001 (2008).
[2] G. R. Tyann, A. Fujisawa, and G. McKee, Plasma Phys. Controlled Fusion **51**, 113001 (2009).
[3] M. Bessendodt-Weberpalset *et al.*, Nucl. Fusion **33**, 1205 (1993).
[4] R. J. Hawryluk, Rev. Mod. Phys. **70**, 537 (1998).
[5] ITER Physics Basis, Nucl. Fusion **39**, 2137 (1999).
[6] H. Yamada *et al.*, Nucl. Fusion **45**, 1684 (2005).
[7] U. Stroth, G. Kühner, H. Maassberg, and H. Ringler (W7-AS Team), Phys. Rev. Lett. **70**, 936 (1993).
[8] H. Yamada *et al.*, Nucl. Fusion **41**, 901 (2001).
[9] U. Stroth *et al.*, Phys. Scr. **51**, 655 (1995).
[10] H. Yamada *et al.*, Fusion Sci. Technol. **46**, 82 (2004).
[11] Y. Takeiri *et al.*, Nucl. Fusion **57**, 102023 (2017).
[12] M. Osakabe *et al.*, Fusion Sci. Technol. **72**, 199 (2017).

[13] S. P. Hirshman and J. C. Whitson, Phys. Fluids **26**, 3553 (1983).
[14] S. Murakami, N. Nakajima, and M. Okamaoto, Fusion Technol. **27**, 256 (1995).
[15] M. Yokoyama *et al.*, Nucl. Fusion **57**, 126016 (2017).
[16] H. Lee, K. Ida, M. Osakabe, M. Yokoyama, C. Suzuki, K. Nagaoka, R. Seki, M. Yoshinuma, and N. Tamura, Plasma Phys. Controlled Fusion **55**, 014011 (2013).
[17] K. Ogawa, M. Isobe, K. Toi, A. Shimizu, D. A. Spong, M. Osakabe, and S. Yamamoto, Nucl. Fusion **50**, 084005 (2010).
[18] J. G. Cordey *et al.*, Nucl. Fusion **39**, 301 (1999).
[19] J. G. Cordey *et al.*, Plasma Phys. Controlled Fusion **42**, A127 (2000).
[20] C. F. Maggi *et al.*, Nucl. Fusion **59**, 076028 (2019).
[21] K. Fujii, M. Goto, and S. Morita, Nucl. Fusion **55**, 063029 (2015).
[22] P. A. Schneider *et al.*, Nucl. Fusion **57**, 066003 (2017).
[23] J. Garcia *et al.*, Nucl. Fusion **59**, 086047 (2019).